Synthesis and Structural and Magnetic Characterization of Ni(Core)/NiO(Shell) Nanoparticles

Aaron C. Johnston-Peck, Junwei Wang, and Joseph B. Tracy*

Department of Materials Science and Engineering, North Carolina State University, Raleigh, North Carolina 27695

ABSTRACT A size series of ligand-stabilized Ni nanoparticles (NPs) with diameters between 8−24 nm was prepared by solution chemistry, followed by solution-phase oxidation with atmospheric oxygen at 200 °C to form Ni(core)/NiO(shell) NPs with shell thicknesses of 2−3 nm. In comparison with the oxidation of Fe and Co NPs, Ni NPs require higher temperatures for significant conversion to NiO. Transmission electron microscopy and electron diffraction show polycrystalline cores with predominantly amorphous shells. SQUID magnetometry measurements were performed to assess the effects of coupling between the ferromagnetic Ni cores and antiferromagnetic NiO shells. After intentional oxidation, the Ni(core)/NiO(shell) NPs have decreased superparamagnetic blocking temperatures (T_B) and no exchange shift (H_{EB}), but a small enhancement in the coercivity (H_C) signifies weak exchange bias. These effects originate from the amorphous structure of the NiO shells and their thin layer thickness that renders the NiO moments incapable of pinning the core moment in moderate applied fields. The magnetocrystalline anisotropy constants before and after oxidation approach the value for bulk Ni and depend on the Ni core size and NiO shell thickness.

KEYWORDS: magnetic nanoparticles · exchange bias · nickel · nickel oxide · superparamagnetism · magnetic anisotropy

Core/shell nanoparticles (NPs) composed of cores and shells with distinctly different compositions can be engineered for special properties that are not available in unary-core NPs. Important examples of useful core/shell NPs include (1) CdSe(core)/ZnS(shell), where the ZnS shell confines excitons to the CdSe, which increases the quantum yield and reduces luminescence from surface traps;[1,2] (2) Fe_3O_4(core)/Au(shell) NPs, where the Au imparts a tunable surface plasmon resonance absorbance and facile surface coupling chemistry through use of thiols;[3] (3) Co(core)/CoO(shell) NPs exhibiting exchange bias,[4−12] an effect in which the antiferromagnetic CoO shells enhance the effective magnetic anisotropy of the Co cores.[13−18] Ferromagnet(core)/antiferromagnet(shell) NPs are of particular interest for their potential to overcome the superparamagnetic limit for ultrahigh-density magnetic recording,[7] to enhance contrast in magnetic resonance imaging,[19] and for potential uses in spintronic devices, such as spin valves.[20]

Here, we report the *solution-phase* synthesis and controlled oxidation of *ligand-stabilized* Ni NPs of different sizes to form Ni(core)/NiO(shell) NPs with different core sizes and shell thicknesses. The magnetic properties of these NPs are of particular interest, because ferromagnetic Ni is converted to antiferromagnetic NiO, which can give rise to exchange bias. Ligand-stabilized NPs may also self-assemble into highly ordered superlattice crystals or films, or they may be biofunctionalized for medical applications.[21] Most of the Ni/NiO NPs previously studied cannot self-assemble or undergo biofunctionalization, because they lack ligand stabilization and are already agglomerated or pinned to surfaces. Detailed structural and magnetic characterization of our Ni(core)/NiO(shell) NPs is presented, and the relationship between the magnetic properties and nanostructure is discussed. Beyond magnetism, there is substantial interest in Ni NPs for catalysis of chemical reactions[22] and growth of carbon nanotubes[23] and nanofibers.[24] NiO has also been used as a hole-transport layer in LEDs.[25]

Exchange bias occurs when a ferromagnet (FM) shares an interface with an antiferromagnet (AFM) having a larger magnetic anisotropy, and the AFM pins the orientation of the moment in the FM layer (through the exchange interaction). Despite vigorous research into the microscopic mechanism of EB since its initial discovery[26] and renewed interest following the advent of spin valves, in which EB can be used to pin one magnetic layer, much understanding of EB at the microscopic level and the factors determining the strength of its pinning interaction remain incomplete. EB is manifested in field-dependent magnetometry

*Address correspondence to jbtracy@ncsu.edu.

Received for review January 8, 2009 and accepted April 02, 2009.

Published online April 10, 2009.
10.1021/nn900019x CCC: $40.75

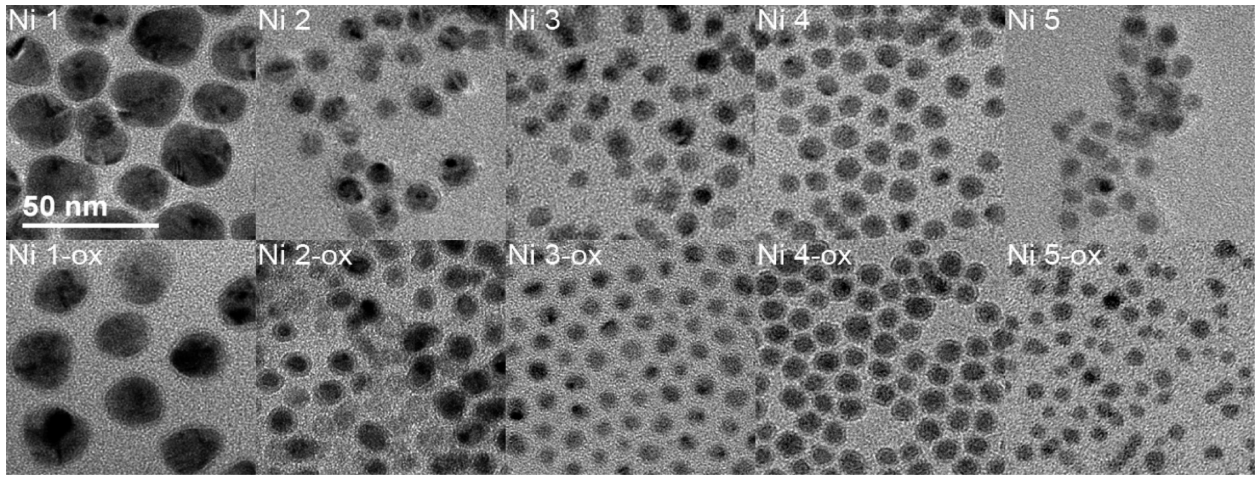

Figure 1. TEM images of Ni nanoparticles: (top row) native samples; (bottom row) oxidized samples.

as an enhanced coercivity (H_C) and an asymmetric shift in the center of the hysteresis loop, the exchange shift (H_{EB}), that depends on the magnitude and direction of an externally applied field during cooling.[4,27] To obtain nonzero H_{EB}, the pinning must be maintained at all field strengths, $H < H_{max}$ that are applied during the measurement of a hysteresis loop. If the pinning fails at an intermediate field, $0 < H_{int} < H_{max}$, then $H_{EB} = 0$, and H_C cannot be enhanced above H_{int}. EB depends on temperature: H_C and H_{EB} usually decrease as temperature increases. EB is not possible above the Néel temperature (T_N) of the AFM, at which the antiferromagnetic moments disorder and become paramagnetic.

Previous studies of Co/CoO[4−12] and $Fe_{x1}O_{y1}/Fe_{x2}O_{y2}$[28−32] NPs and Ni/NiO NPs[33−45] and nanowires[46] have shown that the antiferromagnetic layer can enhance the magnetic anisotropy of the ferromagnet and, in some cases, can stabilize the fixed orientations of ferromagnetic moments to higher temperatures before thermal energy causes the moments' orientations to fluctuate (superparamagnetism). Moreover, oxides of Co, Fe, and Ni can be prepared through oxidation in air (sometimes requiring elevated temperatures). Although oxidized Fe and Co NPs exhibit novel and potentially useful magnetic properties, both systems also have significant limitations: Controlled oxidation of Fe NPs is challenging, owing to the high reactivity of metallic iron and the diverse iron oxide stoichiometries available.[47] Large EB effects are observed in Co/CoO, but T_N for bulk Co of 290 K[16] severely limits its potential for use in devices that operate at room temperature. In contrast, NiO is a candidate for producing useful EB at room temperature, because bulk NiO has T_N of 520 K.[16] Values for T_N are known to depend on the layer thickness; for crystalline NiO thin films of thickness 2 nm, $T_N \approx 400$ K.[48,49] There have also been several reports of the synthesis and magnetic properties of NiO NPs.[22,50−57]

For this investigation, several sizes of Ni(core)/NiO(shell) NPs with diameters of 8−24 nm were synthesized through thermolysis of nickel acetylacetonate in the presence of oleylamine and trioctylphosphine to generate ligand-stabilized Ni NPs.[21] Through controlled oxidation with air, two different NiO shell thicknesses were obtained. Conventional and high-resolution transmission electron microscopy (TEM and HRTEM) measurements reveal narrow size distributions, polycrystalline cores, and amorphous shells. SQUID magnetometry measurements show the effects of size and the NiO shell thickness on the magnetic properties.

RESULTS AND DISCUSSION

Nanoparticle Growth and Oxidation. Each NP size was prepared in a single batch to minimize batch-to-batch variations. After postsynthesis processing to remove high-boiling solvent and excess ligands (performed in the glovebox to minimize oxidation), each batch was split in half. One portion containing "*native*" NPs with minimal oxidation was used as-is. The other half, the *oxidized* sample, was redispersed into dioctyl ether for oxidation by bubbling air through the solution at 200 °C for 4 h.[11,58] Both the native and oxidized samples were dispersed into polymer sticks for SQUID magnetometry measurements[11,59] to minimize the effects of dipolar coupling and thus to measure the magnetic properties of noninteracting NPs. (Photographs of polymer sticks containing Ni NPs are shown in the Supporting Information, Figure S-1.) Several studies have highlighted the importance of a matrix to increase the interparticle distances; without use of a matrix, dipolar coupling contributes to a significant increase in the superparamagnetic blocking temperatures (T_B).[60−64]

Structural Characterization. TEM, HRTEM, and selected-area electron diffraction (SAED) were performed to measure the NP size, to characterize the crystallinity and crystal structure, and to image the NiO shells. Rep-

TABLE 1. Average Ni Core Diameter and NiO Shell Thickness

		native		oxidized	
sample	$d_{total,TEM}$ (nm)	d_{core} (nm)	t_{shell} (nm)	d_{core} (nm)	t_{shell} (nm)
Ni 1	23.8 ± 2.6	22.6	0.6	18.6	2.6
Ni 2	10.3 ± 1.6	7.9	1.2	7.3	1.5
Ni 3	8.2 ± 0.8	6.6	0.8	6.1	1.1
Ni 4	8.8 ± 0.9	6.4	1.2	4.4	2.2
Ni 5	7.6 ± 0.5	5.3	1.1	2.8	2.4

resentative images of each NP sample before (Ni x) and after oxidation (Ni x-ox) treatment (Figure 1) show clearly identifiable NiO shells for several samples. The nonuniform contrast in the TEM images indicates that the cores are polycrystalline, as we have verified by HR-TEM (Supporting Information, Figure S-2) images of the crystal lattice. SAED (Supporting Information, Figure S-3) confirms the particles are face-centered-cubic (fcc) Ni and do not show the presence of any other crystalline phases, including NiO. We note that a synthetic method from which ours is derived (and which is quite similar to ours) is known to lead to amorphous or highly polycrystalline fcc Ni NPs,[22] and others have reported similarly disordered structures.[65−67] TEM and HRTEM further suggest that the NiO shells are mostly amorphous, because we observe crystal lattice only over small regions within the NiO shells, and in conventional TEM, the NiO shells had predominantly uniform contrast. We note that since we cannot measure a lattice parameter for the amorphous oxide, we have not rigorously verified the stoichiometry of the oxide phase as NiO. NiO is, however, the only well-characterized oxide of nickel, which is known to have slight stoichiometric variations from 1:1,[68] and the oxide phase is generally reported as NiO.

NP sizes (Table 1) were determined by manually measuring[69] the diameter of each particle twice and then taking the average value for more than 200 NPs for each native NP sample. Histograms of the NP size distributions are shown in the Supporting Information, Figure S-4. The NiO shell thickness was calculated from a combined TEM measurement of the total NP diameter and the reduction of the saturation magnetization below the bulk value ($M_{S,BulkNi}$), of 57.2 emu/g at 2.5 K,[70] as described in the Supporting Information. (Alternately, the shell thicknesses for most samples can be measured by TEM, but with less accuracy, because Ni NPs on TEM substrate films are more susceptible to oxidation than NP samples for magnetometry measurements that were dispersed in polymers and were stored in a glovebox.)

The native NPs had thin NiO surface layers ranging in thickness (0.6−1.2 nm). After performing intentional oxidation, the NiO shell thickness increased to 1.1−2.6 nm. Extended oxidation times at 200 °C do not increase the shell thickness, which suggests that NiO layers of 2−3 nm thickness form a passivating layer[36] that prevents further oxidation at 200 °C. *In comparison with oxidation of Fe and Co NPs, conversion of Ni to NiO in nanoparticle form requires more driving force*: Fe NPs quickly oxidize upon exposure to air at room temperature.[71] Co NPs can from form Co(core)/CoO(shell) NPs upon room temperature exposure to air[4,11] and can be converted to hollow, crystalline CoO NPs at temperatures below 200 °C.[11,58]

Magnetic Characterization. SQUID measurements (Quantum Design MPMS-XL7 magnetometer) of the temperature- and field-dependent magnetizations of each NP sample, dispersed in the polymer matrix, were acquired to assess the superparamagnetic blocking temperature (T_B), magnetic hysteresis (M_S and H_C), and exchange bias (H_C and H_{EB}). The magnetization units of emu/g are based on the mass of nickel; the mass of oxygen in NiO and of the ligands is excluded.

For each native/oxidized (Ni x/Ni x-ox) pair of samples, the oxidized sample was prepared from the native sample, which eliminated the possibility of batch-to-batch variations and ensured that each pair had the same size (before oxidation) and the same size distribution. The chief aim of the magnetic measurements was to perform pairwise comparison of each oxidized sample (Ni x-ox) with a minimally oxidized reference (Ni x) to discern the effects of oxidation. Comparisons between the whole sets of native and oxidized samples must be interpreted cautiously because of variations of the NiO thicknesses within each set. There is also partial overlap among the native and oxidized samples: Ni 2, Ni 4, Ni 5, Ni 2-ox, and Ni 3-ox all have NiO shell thicknesses of 1.1−1.5 nm.

Measurements of the temperature-dependent magnetization (*M vs T*) acquired in a 100 Oe field during heating after zero-field cooling (ZFC) are shown in Figure 2. At T_B, the ferromagnetic moment within each NP decouples from the crystal lattice and becomes superparamagnetic. For dc SQUID measurements, T_B is typically chosen as $T_B = KV/(25k_B)$, such that the magnetocrystalline anisotropy energy (KV) is much greater than thermal energy, where V is the ferromagnetic core volume.[72] Experimentally, T_B is measured as the temperature corresponding to the peak in *M versus T*: The magnetization reaches a maximum when thermal energy facilitates reorientation of NP moments into the small applied field but is not so large that it randomizes NP moments' orientations. As expected, in our measurements, T_B decreases with decreasing core size, which can be achieved by choosing a greater extent of oxidation or by choosing a batch of NPs with a smaller total diameter.

Measurements of *M versus H* for each sample (Figure 3) were performed at 2.5 K while scanning the field from 50 to −50 kOe, and then back to 50 kOe after cooling from room temperature in 50 kOe field (FC) or zero field (ZFC). Values of M_S and H_C at 2.5 K are reported in

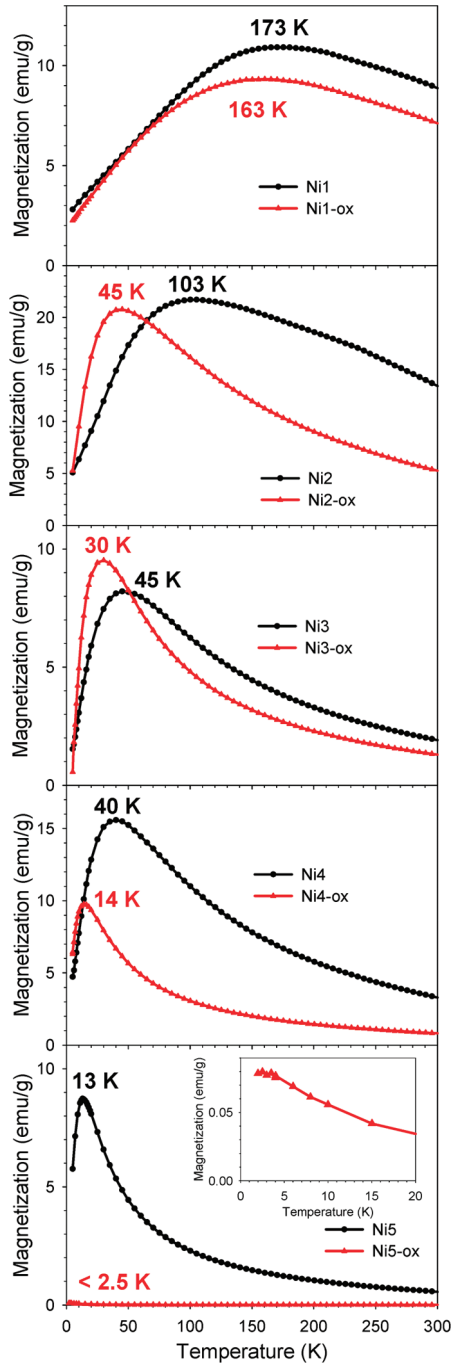

Figure 2. *M vs T* after cooling in zero field for native and oxidized Ni(core)/NiO(shell) NPs. The inset (bottom panel) shows greater detail of the low-temperature region. Labels indicate T_B for each sample.

Table 2, and the size-dependence of H_C is plotted in Figure 4. After applying a linear correction for the diamagnetic magnetization of the polymer, the magnetization for most samples did not saturate asymptotically to a fixed value. At high fields, the slope of *M versus H* was greater for the oxidized samples, because antiferromagnetic NiO magnetizes in the field direction but does not saturate in a 50 kOe field.[22,50−57] The oxidized samples show a greater deviation from ferromagnetic saturation behavior, because they have greater NiO content than the native samples. For calculating the saturation magnetization of the Ni cores ($M_{S,Ni}$), a line of slope k_i was fit to the ZFC magnetization for each sample at high fields, and then a line intersecting the origin with slope $-k_i$ was added to the magnetization to remove the magnetization of NiO. This forced asymptotic saturation behavior at high fields, from which M_S was obtained. For greater extents of oxidation, M_S systematically decreases due to the lower unoxidized Ni content.

For all samples, there is no exchange shift at 2.5 K, even with 50 kOe field cooling, and for each sample except the largest size, H_C is slightly larger after oxidation, which originates from an *enhanced anisotropy consistent with weak exchange bias*. Plots of H_C *versus* d_{core} (Figure 4) also show that for a given core size, H_C is greater with a thicker NiO shell. A comparison of H_C for 50 kOe and zero-field cooling (Table 2) shows rather small differences in H_C, which is consistent with no exchange shift, because the NiO shell is unable to remember any specific pinning orientation. Other studies have shown that NiO NPs of 5 nm diameter have significant H_{EB},[50,73,74] and H_{EB} of 80 Oe at 5 K[38] has been reported for crystalline[36] Ni(core)/NiO(shell) NPs with ~2 nm shells, which suggests that *the reduction in the magnetic anisotropy causing H_{EB} to vanish primarily originates from the amorphous structure of our NiO shells*. A thicker amorphous NiO layer would be needed to provide the same pinning strength as a thinner, crystalline NiO layer, because structural disorder in amorphous NiO reduces its ability to pin the Ni core. However, defects and partial disorder within crystalline antiferromagnets can enhance EB.[13] In a related study of Ni/NiO NPs, EB pinning of the Ni phase originated from coupling with a spin-glasslike, disordered NiO phase.[44]

We have also considered that T_N is reduced for thin layers of NiO, and the amorphous structure could cause a further reduction in T_N. Such lowering of T_N alone is probably insufficient to cause H_{EB} to vanish at 2.5 K. For crystalline NiO films of 2 nm thickness, $T_N \approx 400$ K,[48,49] and structural disorder in the amorphous NiO is expected to further reduce T_N, but $T_N < 2.5$ K for amorphous NiO remains rather unlikely. The absence of an exchange shift at a particular temperature T_0 does not imply $T_N < T_0$. Pinning through EB can fail above T_N if the NiO moments cant or flip when moderate magnetic fields are applied,[13,18,75] or the amorphous NiO shells may be superparamagnetic even at 2.5 K due to a lowered magnetocrystalline anisotropy. We note that K_{NiO} is generally substantially less than K_{CoO}.[76] Therefore, the minimum thickness giving rise to EB at a particular temperature should be thinner for CoO rather than for NiO.[18,77] Indeed, this is the case; prior results show significant EB in Co(core)/CoO(shell) NPs having CoO thicknesses of 3 nm.[11]

The size-dependence of T_B allows for measurements of magnetocrystalline anisotropy constants and an as-

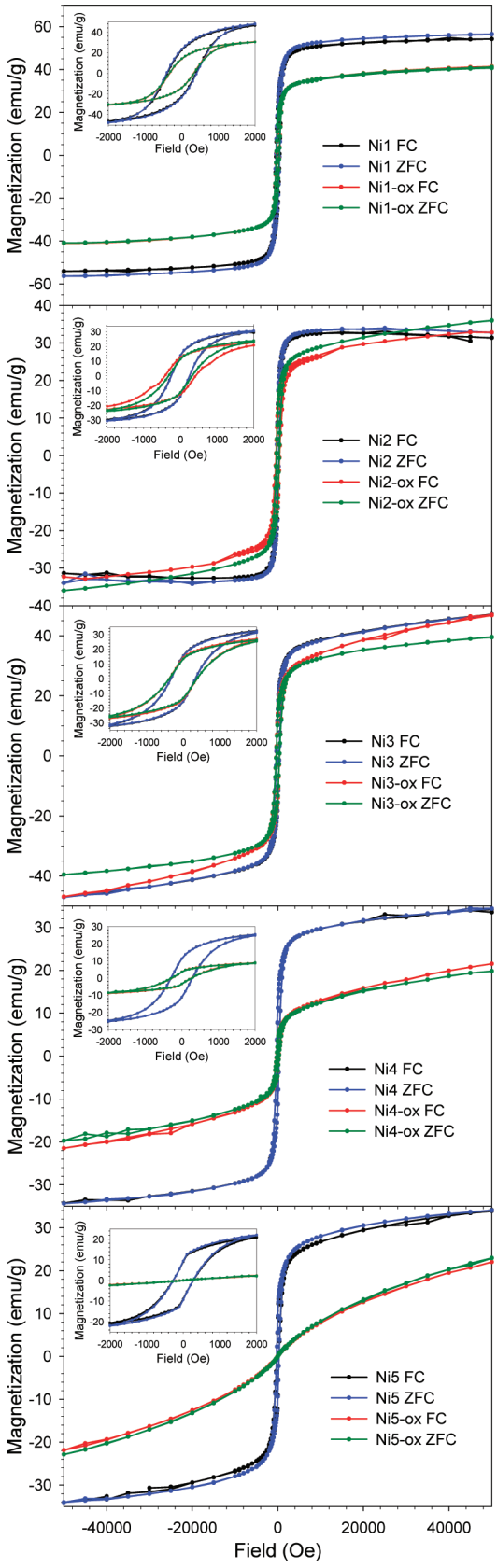

Figure 3. *M vs H* at 2.5 K for native and oxidized Ni(core)/NiO(shell) NPs after cooling from room temperature in 50 kOe field (FC) or zero field (ZFC). Insets show greater detail of the same measurements.

TABLE 2. Saturation Magnetization and Coercivity at 2.5 K with 50 kOe or Zero-Field Cooling

	native			oxidized		
sample	M_s (emu/g)	$H_{C,ZFC}$ (Oe)	$H_{C,FC}$ (Oe)	M_s (emu/g)	$H_{C,ZFC}$ (Oe)	$H_{C,FC}$ (Oe)
Ni 1	52.0	411	390	34.5	334	328
Ni 2	33.7	248	249	27.5	319	319
Ni 3	36.7	332	331	31.1	379	383
Ni 4	28.9	292	291	10.9	274	263
Ni 5	26.8	271	275	4.6	33	30

sessment of the relative strengths of other sources of anisotropy (surface anisotropy[78] and EB). The blocking temperature was previously introduced as $T_B = KV/(25k_B)$ for a system exhibiting magnetocrystalline anisotropy only. To account for surface anisotropy and EB, an additional term, $f(V,T,t_{shell})$, can be added, giving: $T_B = KV/(25k_B) + f(V,T,t_{shell})$. When magnetocrystalline anisotropy is predominant, plots of T_B *versus* V (Figure 5) are expected to be linear and to have slope $KV/(25k_B)$. For these plots, the core volume has been calculated for spheres with the diameters reported in Table 1. The intercept term and sources of nonlinearity are attributed to $f(V,T,t_{shell})$. An important limitation of this analysis is that it assumes K does not depend on temperature, because each blocking temperature is measured when $T = T_B$. The magnetocrystalline anisotropy constants for bulk Ni ($K_{Ni,bulk}$) are known to have a significant temperature dependence (more than an order of magnitude decrease from 2.5 to 300 K).[79] Two other limitations restrict the accuracy of this approach: Higher-order magnetocrystalline anisotropy constants are neglected, and the factor of 25 is an approximation that could be eliminated by performing ac SQUID measurements.[11]

For the native and oxidized samples, T_B *versus* V is linear for all samples except Ni 5 and Ni 5-ox, which are expected to lie below the linear fit, because their blocking temperatures are significantly higher than those for all the other samples, at which K is significantly below its low-temperature value. From linear fits to the four smallest sizes for each sample, we have measured $K_{native} = 1.7 \times 10^6$ erg/cm^3 and $K_{oxidized} = 7.5 \times 10^5$ erg/cm^3. Both of these values agree well with the bulk value, $K_{Ni,bulk} \approx 1 \times$

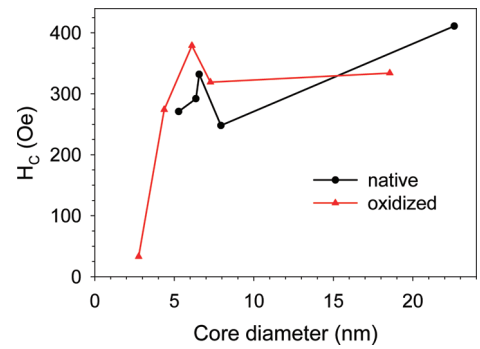

Figure 4. Ni core-size dependence of the coercivity (zero-field cooled).

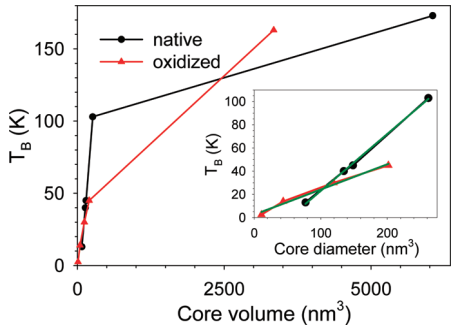

Figure 5. Dependence of T_B on the Ni core volume. Inset shows the same plot, omitting the two data points for samples with the largest volumes (Ni 5 and Ni 5-ox). Linear fits are shown in green.

10^6 erg/cm^3, below 100 K,[79] but it is remarkable that $K_{native} > K_{oxidized}$. In particular, we note that $H_{C,native} < H_{C,oxidized}$ for cores of the same size (except for the largest sizes). This trend for H_C to increase during oxidation while K decreases violates the Stoner−Wohlfarth[80] model for the hysteresis of single-domain ferromagnetic NPs that predicts $H_C = 2K/M_S$. Oxidation appears to reduce the surface anisotropy (lowering K) while increasing the exchange bias (which increases H_C). The linear regressions also have rather different intercept terms on the temperature axis: $T_{0,native} = -26$ K, and $T_{0,oxidized} = 2$ K. The temperature dependence of K and contributions from other anisotropy sources prevent further interpretation of the difference in intercepts.

CONCLUSIONS

In summary, synthetic control over the core size and shell thickness of ligand-stabilized Ni(core)/NiO(shell) NPs has been demonstrated, with maximum shell thicknesses of 2−3 nm. For a given batch of NPs, greater extents of oxidation cause reduction in T_B due to the smaller core volume, but there is also a small enhancement in H_C at low temperature from weak exchange bias that does not cause an exchange shift. The amorphous structure of the NiO shells combined with their thin thickness renders the shells unable to support the interfacial pinning strength necessary for an exchange shift. Magnetocrystalline anisotropy constants for the Ni cores calculated from T_B are consistent with bulk values, but oxidation causes reduced magnetocrystalline anisotropy.

METHODS

Preparation of Ni(Core)/NiO(Shell) Nanoparticles. Our procedure for preparing Ni NPs followed a method reported by the Hyeon group with minor modifications.[21] The NP synthesis was performed using a standard vacuum and inert gas (nitrogen) line and commercially available reagents without further purification. For a typical preparation of 24 nm diameter Ni NPs, 0.2 g nickel acetylacetonate ($Ni(acac)_2$, 98%, TCI) and 2.0 mL oleylamine (97%, Pfaltz & Bauer) were mixed with 5.0 g trioctylphosphine oxide (TOPO, 99%, Strem) and heated to 80 °C in a three-necked, round-bottomed flask for 2 h under vacuum to remove oxygen before backfilling with nitrogen. By syringe, 0.3 mL trioctylphosphine (TOP, 97%, Strem) was injected into the mixture before rapidly heating the solution to 240 °C (in approximately 10 min) with vigorous stirring. After aging the mixture for 30 min at 240 °C, the mixture was cooled to room temperature, and a flocculation procedure was performed to remove the high-boiling solvent and excess ligands: The NPs were first flocculated by adding excess methanol to the solution and then isolated by centrifugation. After discarding the supernatant, three cycles were performed in which the NPs were redispersed in hexanes, precipitated with methanol and centrifuged. The purified NPs were redispersed in toluene and stored in the glovebox to prevent oxidation. The NP sizes can be controlled by adjusting the amounts of $Ni(acac)_2$ and oleylamine. For 10 nm diameter NPs, 0.16 g $Ni(acac)_2$ and 1.6 mL oleylamine was used, and for 8 nm diameter, 0.14 g $Ni(acac)_2$ and 1.4 mL oleylamine was used.

The as-prepared Ni NPs had thin ~1 nm NiO shells. For growth of thicker ~2 nm NiO shells, the NPs were redispersed in dioctyl ether and heated to 200 °C for 4 h while bubbling air through the NP solution.[11,58] The NPs were removed from the high-boiling solvent through flocculation and centrifugation.

Transmission Electron Microscopy. TEM specimens were prepared by placing single drops of dilute NP solutions in hexanes or toluene onto Cu TEM substrates with ultrathin carbon and Formvar support films and allowing the solvent to evaporate. Conventional bright-field imaging and selected-area diffraction were performed using a JEOL 2000FX microscope whose magnification and camera length were calibrated using stained catalase crystals and aluminum, respectively. HRTEM imaging was carried out on a JEOL 2010F microscope.

Polymer Dispersions for Magnetic Measurements. To minimize dipolar interactions between NPs, the NPs were dispersed in monomers that were then polymerized into a matrix of poly(lauryl methacrylate) cross-linked with ethylene glycol dimethacrylate:[11,59] Approximately 10 mg of NPs were dispersed in 1 mL of a solution of 83% lauryl methacrylate, 17% ethylene glycol dimethacrylate, and 0.40% 2,2′-azobisisobutyronitrile (AIBN) by mass. Upon heating the solution to ~110 °C for 5 min, polymerization had occurred. For SQUID measurements, a blank polymer specimen was measured, and the diamagnetic signal was removed from all field-dependent measurements. For determining the magnetization from the measured magnetic moment, inductively coupled plasma-optical emission spectroscopy (ICP-OES) measurements of the concentration of Ni in the polymer were performed by Galbraith Laboratories, Inc.

Acknowledgment. This work was supported by the National Science Foundation (ECCS-0707315) and startup funds from North Carolina State University. We thank Rob Schmidt and David Shultz for access to and assistance with the SQUID magnetometer and Tom Rawdanowicz and Trinity Biggerstaff for TEM training.

Supporting Information Available: Photographs of polymer sticks with and without NPs, HRTEM and electron diffraction of all NP samples, histograms of NP diameter measurements, and details of the calculation of NiO shell thicknesses. This material is available free of charge *via* the Internet at http://pubs.acs.org.

REFERENCES AND NOTES

1. Hines, M. A.; Guyot-Sionnest, P. Synthesis and Characterization of Strongly Luminescing ZnS-Capped CdSe Nanocrystals. *J. Phys. Chem.* **1996**, *100*, 468–471.
2. Dabbousi, B. O.; Rodriguez-Viejo, J.; Mikulec, F. V.; Heine, J. R.; Mattoussi, H.; Ober, R.; Jensen, K. F.; Bawendi, M. G. (CdSe)ZnS Core−Shell Quantum Dots: Synthesis and Characterization of a Size Series of Highly Luminescent Nanocrystallites. *J. Phys. Chem. B* **1997**, *101*, 9463–9475.

3. Xu, Z. C.; Hou, Y. L.; Sun, S. H. Magnetic Core/Shell Fe_3O_4/Au and Fe_3O_4/Au/Ag Nanoparticles with Tunable Plasmonic Properties. *J. Am. Chem. Soc.* **2007**, *129*, 8698–8699.
4. Meiklejohn, W. H.; Bean, C. P. New Magnetic Anisotropy. *Phys. Rev.* **1957**, *105*, 904–913.
5. Gangopadhyay, S.; Hadjipanayis, G. C.; Sorensen, C. M.; Klabunde, K. J. In Exchange-Anisotropy in Oxide-Passivated Co Fine Particles, 37th Annual Conference on Magnetism and Magnetic Materials, Houston, TX, Dec 01−04; Amer Inst Physics: Houston, TX, 1992; pp 6964−6966.
6. Verelst, M.; Ely, T. O.; Amiens, C.; Snoeck, E.; Lecante, P.; Mosset, A.; Respaud, M.; Broto, J. M.; Chaudret, B. Synthesis and Characterization of CoO, Co_3O_4, and Mixed Co/CoO Nanoparticles. *Chem. Mater.* **1999**, *11*, 2702–2708.
7. Skumryev, V.; Stoyanov, S.; Zhang, Y.; Hadjipanayis, G.; Givord, D.; Nogués, J. Beating the Superparamagnetic Limit with Exchange Bias. *Nature (London)* **2003**, *423*, 850–853.
8. Spasova, M.; Wiedwald, U.; Farle, M.; Radetic, T.; Dahmen, U.; Hilgendorff, M.; Giersig, M. In Temperature Dependence of Exchange Anisotropy in Monodisperse Cobalt Nanoparticles with a Cobalt Oxide Shell, International Conference on Magnetism (ICM 2003), Rome, Italy, Jul 27−Aug 01; 2003; pp 1508−1509.
9. Morel, R.; Brenac, A.; Portemont, C. Exchange Bias and Coercivity in Oxygen-Exposed Cobalt Clusters. *J. Appl. Phys.* **2004**, *95*, 3757–3760.
10. Nogués, J.; Sort, J.; Langlais, V.; Doppiu, S.; Dieny, B.; Muñoz, J. S.; Suriñach, S.; Baró, M. D.; Stoyanov, S.; Zhang, Y. Exchange Bias in Ferromagnetic Nanoparticles Embedded in an Antiferromagnetic Matrix. *Int. J. Nanotechnol.* **2005**, *2*, 23–42.
11. Tracy, J. B.; Weiss, D. N.; Dinega, D. P.; Bawendi, M. G. Exchange Biasing and Magnetic Properties of Partially and Fully Oxidized Colloidal Cobalt Nanoparticles. *Phys. Rev. B* **2005**, *72*, 064404.
12. Tracy, J. B.; Bawendi, M. G. Defects in CoO in Oxidized Cobalt Nanoparticles Dominate Exchange Biasing and Exhibit Anomalous Magnetic Properties. *Phys. Rev. B* **2006**, *74*, 184434.
13. Nogués, J.; Sort, J.; Langlais, V.; Skumryev, V.; Suriñach, S.; Muñoz, J. S.; Baró, M. D. Exchange Bias in Nanostructures. *Phys. Rep.* **2005**, *422*, 65–117.
14. Berkowitz, A. E.; Takano, K. Exchange Anisotropy−A Review. *J. Magn. Magn. Mater.* **1999**, *200*, 552–570.
15. Kiwi, M. Exchange Bias Theory. *J. Magn. Magn. Mater.* **2001**, *234*, 584–595.
16. Nogués, J.; Schuller, I. K. Exchange Bias. *J. Magn. Magn. Mater.* **1999**, *192*, 203–232.
17. Stamps, R. L. Mechanisms for Exchange Bias. *J. Phys. D: Appl. Phys.* **2000**, *33*, R247−R268.
18. Iglesias, Ò.; Labarta, A.; Batlle, X. Exchange Bias Phenomenology and Models of Core/Shell Nanoparticles. *J. Nanosci. Nanotechnol.* **2008**, *8*, 2761–2780.
19. Hütten, A.; Sudfeld, D.; Ennen, I.; Reiss, G.; Hachmann, W.; Heinzmann, U.; Wojczykowski, K.; Jutzi, P.; Saikaly, W.; Thomas, G. New Magnetic Nanoparticles for Biotechnology. *J. Biotechnol.* **2004**, *112*, 47–63.
20. Prinz, G. A. Device Physics—Magnetoelectronics. *Science* **1998**, *282*, 1660–1663.
21. Lee, I. S.; Lee, N.; Park, J.; Kim, B. H.; Yi, Y. W.; Kim, T.; Kim, T. K.; Lee, I. H.; Paik, S. R.; Hyeon, T. Ni/NiO Core/Shell Nanoparticles for Selective Binding and Magnetic Separation of Histidine-Tagged Proteins. *J. Am. Chem. Soc.* **2006**, *128*, 10658–10659.
22. Park, J.; Kang, E.; Son, S. U.; Park, H. M.; Lee, M. K.; Kim, J.; Kim, K. W.; Noh, H. J.; Park, J. H.; Bae, C. J.; Park, J. G.; Hyeon, T. Monodisperse Nanoparticles of Ni and NiO: Synthesis, Characterization, Self-Assembled Superlattices, and Catalytic Applications in the Suzuki Coupling Reaction. *Adv. Mater.* **2005**, *17*, 429–434.
23. Huang, Z. P.; Wang, D. Z.; Wen, J. G.; Sennett, M.; Gibson, H.; Ren, Z. F. Effect of Nickel, Iron and Cobalt on Growth of Aligned Carbon Nanotubes. *Appl. Phys. A* **2002**, *74*, 387–391.
24. Guan, Y. F.; Pearce, R. C.; Melechko, A. V.; Hensley, D. K.; Simpson, M. L.; Rack, P. D. Pulsed Laser Dewetting of Nickel Catalyst for Carbon Nanofiber Growth. *Nanotechnology* **2008**, *19*, 235604.
25. Caruge, J. M.; Halpert, J. E.; Bulovič, V.; Bawendi, M. G. NiO as an Inorganic Hole-Transporting Layer in Quantum-Dot Light-Emitting Devices. *Nano Lett.* **2006**, *6*, 2991–2994.
26. Meiklejohn, W. H.; Bean, C. P. New Magnetic Anisotropy. *Phys. Rev.* **1956**, *102*, 1413–1414.
27. Leighton, C.; Nogués, J.; Jönsson-Åkerman, B. J.; Schuller, I. K. Coercivity Enhancement in Exchange Biased Systems Driven by Interfacial Magnetic Frustration. *Phys. Rev. Lett.* **2000**, *84*, 3466–3469.
28. Zheng, R. K.; Wen, G. H.; Fung, K. K.; Zhang, X. X. Giant Exchange Bias and the Vertical Shifts of Hysteresis Loops in γ-Fe_2O_3-Coated Fe Nanoparticles. *J. Appl. Phys.* **2004**, *95*, 5244–5246.
29. Zheng, R. K.; Wen, G. H.; Fung, K. K.; Zhang, X. X. Training Effect of Exchange Bias in γ-Fe_2O_3 Coated Fe Nanoparticles. *Phys. Rev. B* **2004**, *69*, 214431.
30. Ceylan, A.; Baker, C. C.; Hasanain, S. K.; Shah, S. I. Effect of Particle Size on the Magnetic Properties of Core-Shell Structured Nanoparticles. *J. Appl. Phys.* **2006**, *100*, 034301.
31. Martínez-Boubeta, C.; Martínez, B. Critical Radius for Exchange Bias in Naturally Oxidized Fe Nanoparticles. *Phys. Rev. B* **2006**, *74*, 054430.
32. Kavich, D. W.; Dickerson, J. H.; Mahajan, S. V.; Hasan, S. A.; Park, J. H. Exchange Bias of Singly Inverted FeO/Fe_3O_4 Core-Shell Nanocrystals. *Phys. Rev. B* **2008**, *78*, 174414.
33. Yao, Y. D.; Chen, Y. Y.; Hsu, C. M.; Lin, H. M.; Tung, C. Y.; Tai, M. F.; Wang, D. H.; Wu, K. T.; Suo, C. T. Thermal and Magnetic Studies of Nanocrystalline Ni. *Nanostruct. Mater.* **1995**, *6*, 933–936.
34. Yao, Y. D.; Chen, Y. Y.; Tai, M. F.; Wang, D. H.; Lin, H. M. Magnetic Anisotropy Effects in Nano-Cluster Nickel Particles. *Mater. Sci. Eng. A* **1996**, *217*, 281–285.
35. Sako, S.; Ohshima, K.; Sakai, M.; Bandow, S. Magnetic Property of NiO Ultrafine Particles with a Small Ni Core. *J. Vac. Sci. Technol. B* **1997**, *15*, 1338–1342.
36. Sakiyama, K.; Koga, K.; Seto, T.; Hirasawa, M.; Orii, T. Formation of Size-Selected Ni/NiO Core-Shell Particles by Pulsed Laser Ablation. *J. Phys. Chem. B* **2004**, *108*, 523–529.
37. Roy, A.; Srinivas, V.; Ram, S.; De Toro, J. A.; Riveiro, J. M. Effect of Interstitial Oxygen on the Crystal Structure and Magnetic Properties of Ni Nanoparticles. *J. Appl. Phys.* **2004**, *96*, 6782–6788.
38. Seto, T.; Akinaga, H.; Takano, F.; Koga, K.; Orii, T.; Hirasawa, M. Magnetic Properties of Monodispersed Ni/NiO Core-Shell Nanoparticles. *J. Phys. Chem. B* **2005**, *109*, 13403–13405.
39. Yi, J. B.; Ding, J.; Zhao, Z. L.; Liu, B. H. High Coercivity and Exchange Coupling of Ni/NiO Nanocomposite Film. *J. Appl. Phys.* **2005**, *97*, 10K306.
40. Roy, A.; Srinivas, V.; Ram, S.; De Toro, J. A.; Mizutani, U. Structure and Magnetic Properties of Oxygen-Stabilized Tetragonal Ni Nanoparticles Prepared by Borohydride Reduction Method. *Phys. Rev. B* **2005**, *71*, 184443.
41. Liu, X. S.; Meridor, U.; Zhao, P.; Song, G. B.; Frydman, A.; Gedanken, A. The Synthesis and Magnetic Properties of Monodispersed Single-Domain Nickel Nanospheres and Highly Globular Nanostructures of $Ni_{core}NiO_{shell}$. *J. Magn. Magn. Mater.* **2006**, *301*, 13–21.
42. Parada, C.; Morán, E. Microwave-Assisted Synthesis and Magnetic Study of Nanosized Ni/NiO Materials. *Chem. Mater.* **2006**, *18*, 2719–2725.
43. Li, S. D.; Liu, M. M.; Bi, H.; Lü, L. Y.; Zou, W. Q.; Huang, Z. G.; Du, Y. W. The Enhanced Magnetic Properties of Ni Nanocrystallites Induced by the Coupling between Ni/NiO Interfaces. *J. Alloys Compd.* **2006**, *425*, 1–3.

44. Del Bianco, L.; Boscherini, F.; Fiorini, A. L.; Tamisari, M.; Spizzo, F.; Antisari, M. V.; Piscopiello, E. Exchange Bias and Structural Disorder in the Nanogranular Ni/NiO System Produced by Ball Milling and Hydrogen Reduction. *Phys. Rev. B* **2008**, *77*, 094408.
45. Sun, X. C.; Dong, X. L. Magnetic Properties and Microstructure of Carbon Encapsulated Ni Nanoparticles and Pure Ni Nanoparticles Coated with NiO Layer. *Mater. Res. Bull.* **2002**, *37*, 991–1004.
46. Salgueiriño-Maceira, V.; Correa-Duarte, M. A.; Bañobre-López, M.; Grzelczak, M.; Farle, M.; Liz-Marzán, L. M.; Rivas, J. Magnetic Properties of Ni/NiO Nanowires Deposited onto CNT/Pt Nanocomposites. *Adv. Funct. Mater.* **2008**, *18*, 616–621.
47. Redl, F. X.; Black, C. T.; Papaefthymiou, G. C.; Sandstrom, R. L.; Yin, M.; Zeng, H.; Murray, C. B.; O'Brien, S. P. Magnetic, Electronic, and Structural Characterization of Nonstoichiometric Iron Oxides at the Nanoscale. *J. Am. Chem. Soc.* **2004**, *126*, 14583–14599.
48. Abarra, E. N.; Takano, K.; Hellman, F.; Berkowitz, A. E. Thermodynamic Measurements of Magnetic Ordering in Antiferromagnetic Superlattices. *Phys. Rev. Lett.* **1996**, *77*, 3451–3454.
49. Alders, D.; Tjeng, L. H.; Voogt, F. C.; Hibma, T.; Sawatzky, G. A.; Chen, C. T.; Vogel, J.; Sacchi, M.; Iacobucci, S. Temperature and Thickness Dependence of Magnetic Moments in NiO Epitaxial Films. *Phys. Rev. B* **1998**, *57*, 11623–11631.
50. Makhlouf, S. A.; Parker, F. T.; Spada, F. E.; Berkowitz, A. E. Magnetic Anomalies in NiO Nanoparticles. *J. Appl. Phys.* **1997**, *81*, 5561–5563.
51. Kodama, R. H.; Makhlouf, S. A.; Berkowitz, A. E. Finite Size Effects in Antiferromagnetic NiO Nanoparticles. *Phys. Rev. Lett.* **1997**, *79*, 1393–1396.
52. Berkowitz, A. E.; Kodama, R. H.; Makhlouf, S. A.; Parker, F. T.; Spada, F. E.; McNiff, E. J.; Foner, S. In Anomalous Properties of Magnetic Nanoparticles, 7th European Magnetic Materials and Applications Conference (EMMA 98), Zaragoza, Spain, Sep 09−12, 1998; pp 591−594.
53. Kodama, R. H.; Berkowitz, A. E. Atomic-Scale Magnetic Modeling of Oxide Nanoparticles. *Phys. Rev. B* **1999**, *59*, 6321–6336.
54. Li, L.; Chen, L. J.; Qihe, R. M.; Li, G. S. Magnetic Crossover of NiO Nanocrystals at Room Temperature. *Appl. Phys. Lett.* **2006**, *89*, 134102.
55. Bahl, C. R. H.; Mørup, S. Varying the Exchange Interaction between NiO Nanoparticles. *Nanotechnology* **2006**, *17*, 2835–2839.
56. Ghosh, M.; Biswas, K.; Sundaresan, A.; Rao, C. N. R. MnO and NiO Nanoparticles: Synthesis and Magnetic Properties. *J. Mater. Chem.* **2006**, *16*, 106–111.
57. Thota, S.; Kumar, J. Sol-Gel Synthesis and Anomalous Magnetic Behaviour of NiO Nanoparticles. *J. Phys. Chem. Solids* **2007**, *68*, 1951–1964.
58. Yin, Y. D.; Rioux, R. M.; Erdonmez, C. K.; Hughes, S.; Somorjai, G. A.; Alivisatos, A. P. Formation of Hollow Nanocrystals through the Nanoscale Kirkendall Effect. *Science* **2004**, *304*, 711–714.
59. Lee, J.; Sundar, V. C.; Heine, J. R.; Bawendi, M. G.; Jensen, K. F. Full Color Emission from II−VI Semiconductor Quantum Dot−Polymer Composites. *Adv. Mater.* **2000**, *12*, 1102–1105.
60. Frankamp, B. L.; Boal, A. K.; Tuominen, M. T.; Rotello, V. M. Direct Control of the Magnetic Interaction between Iron Oxide Nanoparticles through Dendrimer-Mediated Self-Assembly. *J. Am. Chem. Soc.* **2005**, *127*, 9731–9735.
61. Petit, C.; Taleb, A.; Pileni, M. P. Cobalt Nanosized Particles Organized in a 2D Superlattice: Synthesis, Characterization, and Magnetic Properties. *J. Phys. Chem. B* **1999**, *103*, 1805–1810.
62. Poddar, P.; Telem-Shafir, T.; Fried, T.; Markovich, G. Dipolar Interactions in Two- and Three-Dimensional Magnetic Nanoparticle Arrays. *Phys. Rev. B* **2002**, *66*, 060403.
63. Gross, A. F.; Diehl, M. R.; Beverly, K. C.; Richman, E. K.; Tolbert, S. H. Controlling Magnetic Coupling between Cobalt Nanoparticles through Nanoscale Confinement in Hexagonal Mesoporous Silica. *J. Phys. Chem. B* **2003**, *107*, 5475–5482.
64. Bae, C. J.; Angappane, S.; Park, J. G.; Lee, Y.; Lee, J.; An, K.; Hyeon, T. Experimental Studies of Strong Dipolar Interparticle Interaction in Monodisperse Fe_3O_4 Nanoparticles. *Appl. Phys. Lett.* **2007**, *91*, 102502.
65. Henkes, A. E.; Vasquez, Y.; Schaak, R. E. Converting Metals into Phosphides: A General Strategy for the Synthesis of Metal Phosphide Nanocrystals. *J. Am. Chem. Soc.* **2007**, *129*, 1896–1897.
66. Winnischofer, H.; Rocha, T. C. R.; Nunes, W. C.; Socolovsky, L. M.; Knobel, M.; Zanchet, D. Chemical Synthesis and Structural Characterization of Highly Disordered Ni Colloidal Nanoplarticles. *ACS Nano* **2008**, *2*, 1313–1319.
67. Nunes, W. C.; De Biasi, E.; Meneses, C. T.; Knobel, M.; Winnischofer, H.; Rocha, T. C. R.; Zanchet, D. Magnetic Behavior of Ni Nanoparticies with High Disordered Atomic Structure. *Appl. Phys. Lett.* **2008**, *92*, 183113.
68. Greenwood, N. N.; Earnshaw, A. *Chemistry of the Elements*, 2nd ed.; Butterworth-Heinemann: Boston, MA. 1997; 1151–1152.
69. Rasband, W. S. Imagej. http://rsb.info.nih.gov/ij/ (accessed November 1, 2008).
70. O'Handley, R. C. *Modern Magnetic Materials: Principles and Applications*; Wiley-Interscience: New York, 2000; p 99.
71. Peng, S.; Wang, C.; Xie, J.; Sun, S. H. Synthesis and Stabilization of Monodisperse Fe Nanoparticles. *J. Am. Chem. Soc.* **2006**, *128*, 10676–10677.
72. Bean, C. P.; Livingston, J. D. Superparamagnetism. *J. Appl. Phys.* **1959**, *30*, 120S–129S.
73. Bi, H.; Li, S. D.; Zhang, Y. C.; Du, Y. W. Ferromagnetic-Like Behavior of Ultrafine NiO Nanocrystallites. *J. Magn. Magn. Mater.* **2004**, *277*, 363–367.
74. Makhlouf, S. A.; Al-Attar, H.; Kodama, R. H. Particle Size and Temperature Dependence of Exchange Bias in NiO Nanoparticles. *Solid State Commun.* **2008**, *145*, 1–4.
75. Dobrynin, A. N.; Temst, K.; Lievens, P.; Margueritat, J.; Gonzalo, J.; Afonso, C. N.; Piscopiello, E.; Tendeloo, G. V. Observation of Co/CoO Nanoparticles Below the Critical Size for Exchange Bias. *J. Appl. Phys.* **2007**, *101*, 113913.
76. Gruyters, M. Structural and Magnetic Properties of Transition Metal Oxide/Metal Bilayers Prepared by in Situ Oxidation. *J. Magn. Magn. Mater.* **2002**, *248*, 248–257.
77. Lund, M. S.; Macedo, W. A. A.; Liu, K.; Nogués, J.; Schuller, I. K.; Leighton, C. Effect of Anisotropy on the Critical Antiferromagnet Thickness in Exchange-Biased Bilayers. *Phys. Rev. B* **2002**, *66*, 054422.
78. Yanes, R.; Chubykalo-Fesenko, O.; Kachkachi, H.; Garanin, D. A.; Evans, R.; Chantrell, R. W. Effective Anisotropies and Energy Barriers of Magnetic Nanoparticles with Néel Surface Anisotropy. *Phys. Rev. B* **2007**, *76*, 064416.
79. Stearns, M. 3d, 4d and 5d Elements, Alloys and Compounds. In *Landolt-Börnstein—Group III Condensed Matter*; Wijn, H. P. J., Ed.; Springer-Verlag: New York, 1986; Vol. 19a, pp 41−47.
80. Stoner, E. C.; Wohlfarth, E. P. A Mechanism of Magnetic Hysteresis in Heterogeneous Alloys. *Philos. Trans. R. Soc. London, A* **1948**, *240*, 599–642.